Neuron, Vol. 41, 767–779, March 4, 2004, Copyright ©2004 by Cell Press

Plastic and Nonplastic Pyramidal Cells Perform Unique Roles in a Network Capable of Adaptive Redundancy Reduction

Joseph Bastian,[1,*] Maurice J. Chacron,[2,3] and Leonard Maler[2]

[1]Department of Zoology
University of Oklahoma
Norman, Oklahoma 73019

[2]Department of Cellular and Molecular Medicine

[3]Department of Physics
University of Ottawa
Ontario K1N 6N5
Canada

Summary

Pyramidal cells show marked variation in their morphology, including dendritic structure, which is correlated with physiological diversity; however, it is not known how this variation is related to a cell's role within neural networks. In this report, we describe correlations among electrosensory lateral line lobe (ELL) pyramidal cells' highly variable dendritic morphology and their ability to adaptively cancel redundant inputs via an anti-Hebbian form of synaptic plasticity. A subset of cells, those with the largest apical dendrites, are plastic, but those with the smallest dendrites are not. A model of the network's connectivity predicts that efficient redundancy reduction requires that nonplastic cells provide feedback input to those that are plastic. Anatomical results confirm the model's prediction of optimal network architecture. These results provide a demonstration of different roles for morphological/physiological variants of a single cell type within a neural network performing a well-defined function.

Introduction

Central neurons of a given morphological class, such as cortical or hippocampal pyramidal cells, show enormous morphological and biochemical variability (Bannister and Larkman, 1995; Larkman and Mason, 1990). This diversity is correlated with numerous physiological properties including cable structure, ion channel distributions, spontaneous firing patterns and dendritic spiking, burst production, and the ability to detect coincident synaptic inputs (for reviews, see Haüsser and Mel, 2003; Koch and Segev, 2000; Segev and London, 2000), as well as the presence of intracellular signaling systems associated with synaptic plasticity (Jones et al., 1994). Despite detailed understanding of the dependence of physiological properties on neuronal structure, specific roles for different morphological variants within a given cell class have yet to be discovered. Understanding the roles of single neurons in terms of the overall function of specific networks remains a major challenge (Haüsser et al., 1999), and studies exploiting relatively simple systems, with well-described organization and information-processing capabilities, are likely to speed progress toward this goal.

Pyramidal cells within the primary electrosensory processing region, the electrosensory lateral line lobe (ELL) of South American weakly electric fish, were studied. These cells are subdivided into two broad morphological categories; basilar and nonbasilar cells distinguishable by the presence and absence of basilar dendrites (Maler, 1979). The former, also known as E cells, receive direct electroreceptor afferent input and respond to increased afferent activity with excitation. The nonbasilar cells, I cells, are driven disynaptically via inhibitory interneurons and respond to increased afferent input with inhibition (Maler et al., 1981; Saunders and Bastian, 1984). Thus, these cells are functionally similar to retinal On and Off ganglion cells. Previous work showed that both cell types are highly variable in their dendritic structure. This variation is negatively correlated with spontaneous firing frequency and adaptation time constant (Bastian and Courtright, 1991) but positively correlated with the propensity for burst-like firing (Bastian and Nguyenkim, 2001). The biophysics of bursting is well understood (Doiron et al., 2002; Lemon and Turner, 2000). Receptive field organization also varies with dendritic morphology as does the ability to encode the temporal characteristics of naturalistic stimuli (Bastian et al., 2002). In addition, pyramidal cells vary in their expression of intracellular messaging machinery associated with synaptic plasticity (Berman et al., 1995; Zupanc et al., 1992). Thus, these electrosensory neurons provide an excellent model for studies of how morphological and physiological variation within a neuronal category contributes to the information processing capabilities of a well-defined network.

Weakly electric fish generate a continuous quasisinusoidal electric organ discharge (EOD) producing an electric field around the body, which they monitor with electroreceptors scattered over the body surface. Objects in the environment distort the EOD field, providing information useful for electrolocation or prey detection (Bastian, 1986a; Nelson and MacIver, 1999). Changes in the animal's posture, as occur when the animals explore the environment, also result in large changes in EOD field strength and electroreceptor activity, which could interfere with electrolocation (Bastian, 1999). These reafferent inputs are predictable, and an adaptive mechanism, which utilizes electrosensory feedback as well as proprioceptive signals related to posture, cancels responses to these redundant stimuli (Bastian, 1995). An LTD-like form of anti-Hebbian plasticity at the apical dendritic synapses underlies the cancellation mechanism in this and other species (for reviews, see Bell et al., 1997; Bell, 2001).

The discharges of other electric fish also modulate the amplitude of the EOD field, providing electrocommunication information (Hagedorn and Heiligenberg, 1985). Responses to the periodic beat patterns resulting from the interaction of multiple EODs are also attenuated by the cancellation mechanism. In this case, however, cancellation must rely on electrosensory feedback

*Correspondence: jbastian@ou.edu

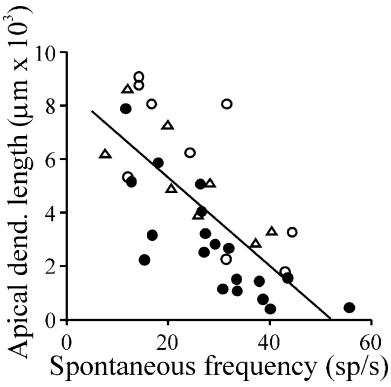

Figure 1. Correlations of Pyramidal Cell Dendritic Size with Spontaneous Firing Frequency

Open circles and triangles indicate E and I cells filled and reconstructed in this study. Filled circles indicate E cells filled and reconstructed previously. Best-fit line is given by dendritic length = 8613 − 145 × spontaneous rate ($r = -0.73$, all data, $n = 36$).

alone, since there are no proprioceptive signals related to the stimulus. Importantly, since all electrosensory information is initially processed by ELL pyramidal cells, the electrosensory feedback used for cancellation could itself be modified as cancellation proceeds. The consequences of such modifiable feedback on the cancellation mechanism are not well understood. Here we describe the relationship between pyramidal cell apical dendritic morphology and plasticity at synapses that convey sensory feedback information to these same cells. We show that the ability to perform this cancellation is highly correlated with the size of a cell's apical dendrite and that cells with the smallest dendrites are not plastic. Based on well-characterized circuitry (Maler et al., 1982; Sas and Maler, 1987), we constructed a network model to test the effects of having the feedback fluctuate as adaptive cancellation proceeds. The model predicts that nonplastic cells are required for the cancellation to occur. Furthermore, the efficiency of the cancellation is maximized if the feedback to the plastic cells is driven exclusively by the nonplastic neurons. Anatomical studies verified the models prediction that input to the higher-order source of this feedback is predominantly from morphologically identified nonplastic cells.

Results

Pyramidal Cell Spontaneous Firing Frequencies and Responses to Amplitude Modulations Covary with Apical Dendritic Structure

An earlier study established a strong negative correlation between pyramidal cell apical dendrite size and spontaneous firing frequency ($r = -0.78$, $p < 0.001$; Bastian and Courtright, 1991). Spontaneous firing frequency refers to activity in the presence of the normal unmodulated EOD. The summed apical dendritic lengths of the 19 E cells from this earlier study (filled circles) along with the dendritic lengths of an additional 9 E (open circles) and 8 I (open triangles) cells filled in the current study are plotted as a function of spontaneous rate (Figure 1). The strong correlation seen in the earlier study is verified by the more recent data ($r = -0.74$, $p = 0.001$, open symbols only), and no differences were seen contingent upon cell type (E versus I). Thus, pyramidal cells will be used to refer to these neurons generally, but E or I cells will be used when referring to specific types. The relationship between spontaneous firing rate and apical dendritic size (regression line of Figure 1) allows estimates of dendritic morphology to be inferred from measures of spontaneous activity recorded with extracellular techniques, which are less likely to damage cells and alter responses.

Responses to naturalistic stimulation patterns, such as sinusoidal amplitude modulations (SAMs) of the EOD, are also correlated with dendritic size. Phase histograms of large-dendrite pyramidal cell responses to SAM stimuli, presented to the entire fish (global geometry), are typically flat (Figure 2A), but the activity of small-dendrite cells is always strongly modulated by this stimulus (Figure 2B). Vector strength, which ranges from 0 to 1 (0 indicating random relationship and 1 indicating perfect phase locking to the stimulus) was used to quantify responses to SAMs. This measure was negatively correlated with dendritic size (Figure 2C, $r = -0.73$, $n = 44$, $p < 0.001$).

The negative correlation relating responsiveness to global SAMs and apical dendrite size may reflect differences among pyramidal cells' receptive fields (RFs). Previous work showed that cells with small apical dendrites had relatively small surround areas compared to the centers of their antagonistic center-surround RFs (Bastian et al., 2002). Their responsiveness to global stimuli may, at least in part, be a consequence of poor common mode rejection due to unbalanced RF centers and surrounds. The unresponsiveness of large-dendrite cells suggests that the efficacy of their RF centers and surrounds are better matched. However, the apparent close match of center-surround efficacy requires functional feedback inputs to these cells. Pharmacological blockade of this feedback renders large-dendrite cells highly sensitive to global stimuli (Figure 4C; Bastian, 1996a). Stimulation of RF centers alone evokes strong responses for both large- and small-dendrite cells (Bastian et al., 2002).

Pyramidal Cell Adaptive Plasticity and Dendritic Structure

Pyramidal cells adaptively cancel predictable patterns of afferent electrosensory input via an anti-Hebbian form of synaptic plasticity. To gauge a cell's ability to perform this cancellation, single neuron responses to global SAM stimuli were compared before and after a "training session" in which the inputs to the RF center and surround were deliberately unbalanced. A small stimulation dipole was positioned 1 to a few mm lateral to the fish's skin within the RF center. SAM stimuli applied via this local dipole in conjunction with the global SAM (G+L stimulation) alters the relative intensity of RF center and surround stimulation. Plastic cells adjust the strength of synaptic input to their apical dendrites in the direction that minimizes responses to this new afferent input pattern.

As expected, large-dendrite cells respond weakly, if at all, to initial presentations of a global SAM stimulus

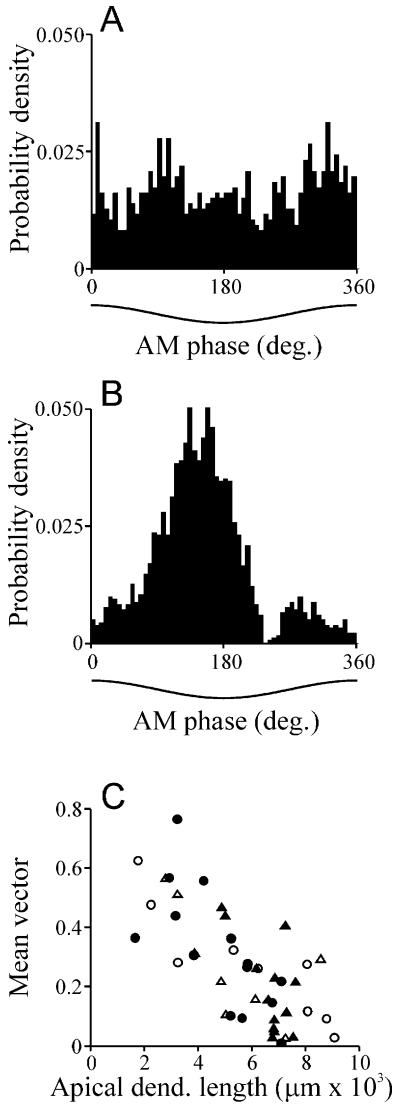

Figure 2. Pyramidal Cell Responses to Global Sinusoidal AMs Are Correlated with Apical Dendritic Size

(A and B) Phase histograms summarizing a low-frequency (13.2 spikes/s) and high-frequency (40.2 spikes/s) E cells' responses to 4 Hz SAM stimuli, respectively. Vector strengths for these histograms are 0.06 ($p = 0.1$) and 0.55 ($p < 0.001$), respectively. p values determined via the Rayleigh statistic (Batschelet, 1981).

(C) Scatter plot relating pyramidal cell responsiveness, measured as the phase histogram mean vector, to the apical dendritic size measured from filled cells (open symbols) or inferred from the relationship of spontaneous firing rate to dendritic size (filled symbols). Circles and triangles indicate data from E ($n = 23$) and I ($n = 21$) cells, respectively.

(Figures 3A1 [G1] and 3A2). Addition of the local stimulus to the RF center evoked strong responses during the positive-going phase of the SAM as expected for E cells (Figures 3A1 [G+L] and 3A3). Following 400 presentations of the G+L stimulus, both were turned off for 20 s to allow the cell to recover from the short-term effects of the strong stimulation. Cells showed a fall in activity immediately following the G+L stimulus but spontaneous activity typically recovered to normal within 20 s. Following this, reapplication of the initially ineffective global stimulus caused strong responses (compare Figures 3A2 and 3A4). Importantly, the phase of the cell's response was opposite that expected for E cells, which are normally driven by increasing, not decreasing, EOD amplitude. Responses following such paired stimulation, termed negative image responses (Bell et al., 1997), are due to changed apical dendritic synaptic strengths designed to cancel the G+L stimulus and are typically 180° out of phase with responses to the G+L stimulus. With continued global stimulation, cells gradually revert to their initial unresponsive state. In the absence of continuous global stimulation, negative image responses persist for at least 30 min (Bastian, 1996a). If during G+L stimulation the local stimulus is presented in antiphase relative to the global, plastic changes develop in a similar fashion but the polarity of the negative image response is inverted and therefore appropriate for canceling this pattern of the G+L stimulus (Figures 3A5–3A8). Earlier studies verified that strong local stimuli applied to the RF center alone fail to cause plastic changes in pyramidal cell responses (Bastian, 1995, 1996a, 1996b).

Strong local stimuli, which increased the stimulus amplitude within the RF center about 5-fold, were used in these experiments to evoke the largest plastic changes that the cell was capable of producing. Hence, little to no change in responses was seen over the duration of the G+L stimulation, because the evolving negative image inputs were insufficient to cancel the strong RF center stimulation. With less intense local stimuli (2–3× increases at the RF center), a gradual loss of responsiveness to the G+L stimulus is seen (Figure 7A1; Bastian, 1995, 1996a).

Reconstruction of this cell revealed the typical morphology of E cells found superficially in the ELL pyramidal cell layer (Figure 3A9). This neuron, located in the most lateral region of the ELL, extended a long basilar dendrite into the ELL deep fiber layer (df) where receptor afferents terminate. Its complex apical dendrite (summed length of dendritic branches = 9072 μm) traversed the full extent of the overlying dorsal and ventral molecular layers (DML, VML). The ELL laminae are highly compressed in this lateral region, and this cell was distorted in the dorsoventral dimension compared to neurons from more medial regions of the ELL (see Figure 8B). The basilar dendrite had a more sinuous appearance than typical, and the apical dendritic tree became highly compressed as it coursed through the superficial regions of the DML.

Cells with the smallest apical dendrites not only respond strongly to initial presentations of global stimuli but also fail to adaptively cancel novel stimulus patterns (Figures 3B1–3B9). This cell (dendritic length = 1788 μm) responded as strongly to the G+L stimulus as did the large-dendrite cell; however, no negative image responses were seen following G+L stimulation (compare Figures 3B2 and 3B4). Likewise, no negative image responses were seen following global plus local stimuli in antiphase (Figures 3B5–3B8). This cell (Figure 3B9) was found deep within the pyramidal cell layer (pyr), and the small apical dendrite consisted of fewer branches that were restricted to the ventral 50% of the DML.

Plastic changes caused by the training paradigm were quantified by computing the vector difference between phase histograms of each cell's response to 100 repli-

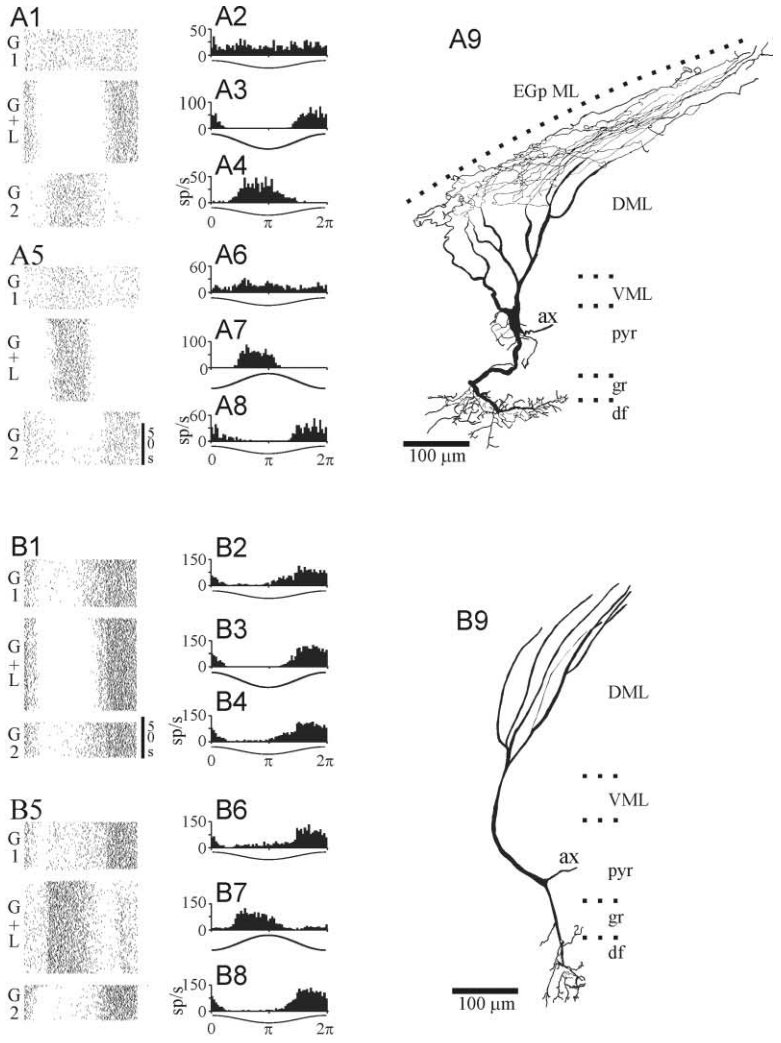

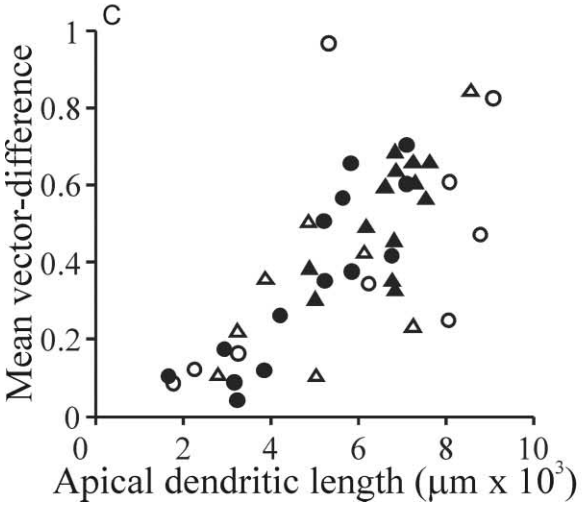

Figure 3. Contrasting Physiology and Morphology of Plastic and Nonplastic E Cells

(A1) Raster display of spike times during initial presentation of global stimulus (G1), during paired global plus local stimuli (G+L), and global stimuli beginning 20 s after the termination of the G+L stimulation (G2).

(A2) Phase histograms of responses to 100 replicates of the initial global stimulus, G1 (mean vector = 0.04, $p = 0.7$).

(A3) Responses to the first 100 replicates of the G+L stimulus.

(A4) Responses to the first 100 replicates of the second presentation of the global stimulus, G2 (mean vector = 0.7, $p < 0.001$).

(A5–A8) Raster display (A5) and phase histograms (A6–A8) summarizing responses of this same cell before, during, and after stimulation with global plus local SAMs in antiphase. Vector strengths of A6 and A8 are 0.16 ($p = 0.001$) and 0.71 ($p < 0.001$), respectively.

(A9) Reconstruction of this E cell (15.2 sp/s spontaneous rate).

(B1–B8) Responses of a nonplastic E cell to the same stimulus paradigm as in (A1)–(A8). Vector strengths for (B2) and (B4) are 0.63 and 0.64. Vector strengths for (B6) and (B8) are 0.65 and 0.68 (p values all <0.001).

(B9) Reconstruction of this E cell (42.9 sp/s spontaneous rate).

Abbreviations: ax, axon; df, deep fiber; DML, dorsal molecular layer of the ELL; EGp ML, molecular layer of the posterior eminentia granularis; gr, granule cell layer; pyr, pyramidal cell layer; VML, ventral molecular layer.

(C) Apical dendritic length predicts the strength of adaptive plasticity. Open circles and triangles are data from E and I cells, respectively, filled and reconstructed ($r = 0.62$, $p = 0.008$, $n = 17$). Filled symbols, extracellularly recorded data ($r = 0.85$, $p < 0.001$, $n = 27$).

cates of the global stimulus immediately preceding and following the G+L stimulation. For most cells, means of these vector differences were computed from two replicates with the local stimulus in-phase during the G+L stimulus plus two replicates with the local stimulus in antiphase. The vector differences for the cells of Figures 3A and 3B averaged 0.83 and 0.09, respectively; the former was highly plastic but the latter was not.

Figure 3C shows that plasticity, measured as mean vector difference, is positively correlated with apical dendritic size ($r = 0.72$, $n = 44$, $p < 0.001$). Although plasticity is clearly graded over a large range, several measures indicate that the subset of cells with the smallest dendrites comprise a nonplastic population. The chi-square test was used to compare phase histograms of responses preceding and following the G+L stimulation (Batschelet, 1981). Cells with dendritic lengths greater than about 4000 μm all showed highly statistically significant changes in response, while those with dendrites smaller than this did not typically show significant changes. Previous work showed that pyramidal cells' tendency to produce spike bursts was also correlated with dendritic size, with a subset of cells having the smallest apical dendrites being nonbursty (Bastian and Nguyenkim, 2001). Cells of this study also fell into two groups depending on whether or not they showed statistically significant spontaneous bursting. Mean dendritic size of nonbursty cells ($\bar{x} = 3801$ μm, SE = 609 μm, $n = 10$) was significantly smaller than that of bursty cells ($\bar{x} = 6216$ μm, SE = 275 μm, $n = 34$; $p = 0.004$, t test). Additionally, the nonbursty cells' mean vector differences were significantly less than those of bursty cells ($\bar{x} = 0.24$, SE = 0.05 and $\bar{x} = 0.47$, SE = 0.04, respectively; $p = 0.002$, t test). Thus, pyramidal cells can be described as being plastic or nonplastic. The nonplastic category is characterized by their nonbursting physiology and very small apical dendrites. Plastic cells are bursty, have larger dendrites, and their ability to cancel redundant inputs is graded with dendritic size.

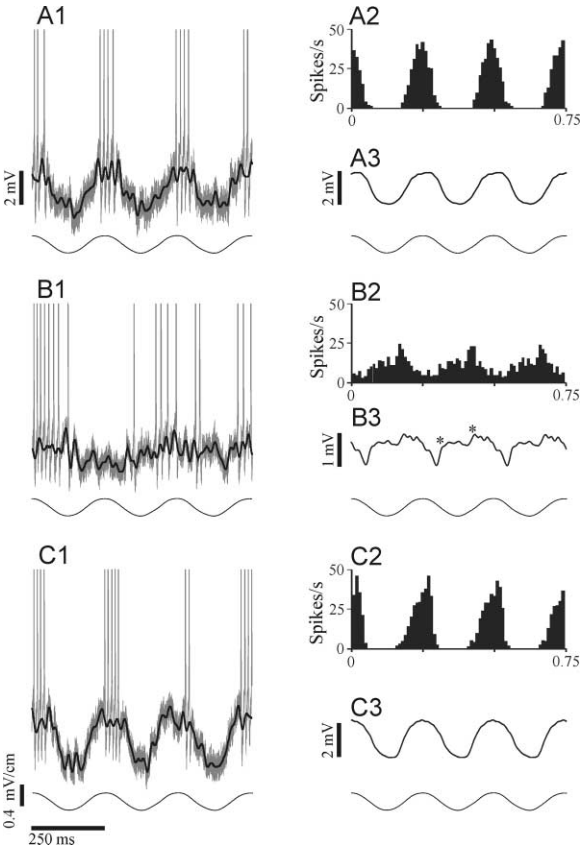

Figure 4. Identification of Membrane Potential Changes Evoked by Synaptic Input to Apical Dendrites

Membrane potential and spike rate changes in response to local stimulation (A1–A3), global stimulation (B1–B3), and global stimulation with CNQX blockade of descending input to apical dendrites (C1–C3). (A1), (B1), and (C1) show raw spike records (truncated), and black lines show membrane potential following spike removal and low-pass filtering. Lower traces show envelope of the SAM stimulus. Calibration of C1 lower trace holds for all SAM envelopes. (A2), (B2), and (C2) are histograms of spike rate measured over 135 SAM cycles in three cycle epochs with local, global, and global stimulation in the presence of CNQX, respectively. (A3), (B3), and (C3) are averages of Vm computed over the same time periods as the spike rate histograms. Asterisks of (B3) indicate transient depolarizations linked to ascending and descending inputs to pyramidal cells.

Membrane Potential Changes Associated with Adaptive Plasticity

Functional apical dendritic synaptic input is necessary for adaptive plasticity (Bastian, 1996a, 1996b). We therefore tested the hypothesis that the small-dendrite cells' lack of plasticity was simply a consequence of insufficient or ineffective feedback input to their dendrites. First, intracellular responses to local were compared with responses to global stimuli. Local stimuli principally activate receptor afferent input to the RF center. Global stimuli activate inputs to RF center as well as the surround recruiting feedback input to the apical dendrites. Thus, comparison of the pattern of membrane potential (Vm) change due to global versus local stimulation should help identify the effects of apical dendritic input (Figure 4). Patterns of Vm change were then analyzed to determine if nonplastic cells differ from those showing robust plasticity in ways that indicate weaker apical dendritic inputs (Figure 5).

Spikes were removed from intracellular records by replacing Vm values over the duration of each spike with the mean of values immediately preceding and following each spike. The records, absent spikes, were then low-pass filtered (0 to 100 Hz, 8th order Butterworth). A sample of the original spike record from an E cell (gray trace) along with the low-pass filtered Vm record (black line) during local RF center stimulation is shown in Figure 4A1. The period histogram (Figure 4A2) and Vm averaged over epochs of three consecutive SAM cycles (Figure 4A3) shows that the cell preferentially fired during the rising phase of the EOD AM and that Vm accurately tracks the stimulus envelope. This Vm pattern reflects primary afferent input to the cell's basilar dendrite. Stimulation with a global SAM stimulus of equivalent amplitude measured at the RF center evoked a weaker pattern of Vm change (Figure 4B1) and spike responses (Figure 4B2). Global stimuli also evoked a more complex pattern of Vm change that deviated from the envelope of the AM; depolarizing transients occur in response to both the rising and falling phases of the AM (Figure 4B3, asterisks).

To determine the degree to which apical dendritic inputs contribute to the changed Vm pattern due to global stimulation, micropressure injection of the non-NMDA glutamate antagonist CNQX was used to block excitatory synaptic transmission within the ELL molecular layers. This technique results in highly localized

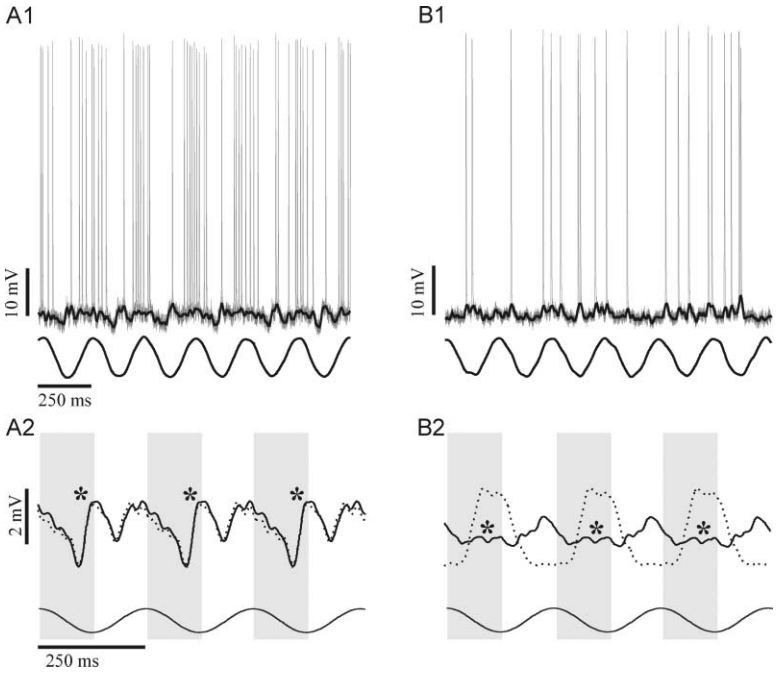

Figure 5. High- and Low-Frequency Pyramidal Cells Show Biphasic Patterns of Vm Change in Response to Global Stimuli

(A1 and B1) Original spike records (gray) and low-passed Vm records with spikes removed (black) during global stimulation. Lower traces show EOD SAM envelope. Spontaneous firing frequency and dendritic length of the cell of A1 was 31.4 spikes/s and 2257 μm and that of A2 was 15.2 spikes/s and 9072 μm.

(A2 and B2) Solid lines are averages of Vm changes during global stimulation prior to paired global plus local stimulation. Dotted lines are averages of Vm changes in response to global stimuli following G+L stimulation. Time calibration of (A1) holds for (B1) and that of (A2) holds for (B2). EOD SAM peak-to-peak amplitude of (A1), (A2) and (B1), (B2) were 0.15 and 0.125 mV/cm, respectively.

blocks of dendritic input (Bastian, 1993). Spike responses (Figure 4C2) and patterns of Vm change (Figures 4C1 and 4C3) evoked by global stimuli in the presence of CNQX were similar to those evoked by local stimulation. Thus, both depolarizing transients associated with the global AM falling phase as well as the reduced response to primary afferent input can be attributed to feedback to the apical dendrites. Similar results were obtained with I cells. In these cases the responses to local stimulation occurred during the falling phase of the SAM, global stimuli resulted in a biphasic pattern of Vm change, and CNQX caused responses to global stimuli to revert to those evoked by local stimuli.

Comparison of large-dendrite and small-dendrite cells' responses to global stimuli shows that complex patterns of Vm change occur for both types. Spike responses of small-dendrite cells (Figure 5A1) are more strongly coupled to the envelope of the EOD AM, and the magnitude and periodicity of the Vm changes are also more pronounced as compared to large-dendrite cells (Figure 5B1). Averages of the Vm records show that the small-dendrite cell responded with larger Vm changes than did the large dendrite cell during the phase of the stimulus that evokes feedback electrosensory input (compare Figures 5A2 and 5B2, solid lines, asterisks). The dotted lines of Figures 5A2 and 5B2 show the Vm patterns evoked by global stimuli after G+L training. This treatment had no effect on the Vm pattern recorded from the small-dendrite cell; however, following G+L stimulation of the large-dendrite cell, the initially small transient reflecting descending inputs was greatly increased, and the transient associated with receptor afferent inputs was attenuated.

Analysis of Vm changes refutes the idea that the lack of plasticity displayed by small-dendrite cells is due to insufficient feedback input. Instead, feedback input may be relatively stronger for cells with smaller dendrites. Peak-to-peak changes in membrane potential evoked by global stimulation increased with decreasing apical dendritic size ($r = -0.56$, $n = 16$, $p = 0.02$). In addition, the change in Vm due to ascending input was also negatively correlated with dendritic length ($r = -.43$, $n = 16$, $p = 0.1$), as was the Vm transient resulting from feedback inputs ($r = -0.46$, $n = 16$, $p = 0.08$). Although these latter two correlations were not statistically significant, the overall trend indicates that both ascending and descending inputs cause larger changes in Vm in cells, with smaller dendritic arbors possibly reflecting higher input resistances of these neurons. The small-dendrite cells' lack of plasticity, therefore, probably reflects their lack of critical intracellular signaling systems (Berman et al., 1995; Zupanc et al., 1992) rather than ineffective apical dendritic inputs.

Nonplastic Pyramidal Cells Are Necessary for Efficient Adaptive Cancellation

In order for adaptive cancellation to occur, there must be a pattern of excitatory and/or inhibitory synaptic input to the pyramidal cells' apical dendrites temporally related to the afferent input to be cancelled. In the case of reafferent stimuli, such as result from changes in an animal's posture, proprioceptive as well as descending electrosensory information is available. Since the non-electrosensory inputs are not affected by the cancellation mechanism, the signal available at the apical dendrites can remain at least partly unchanged as cancellation proceeds. However, the cancellation of electrosensory inputs alone, described above, relies solely on electrosensory feedback. The effects of having the electrosensory feedback signal itself sensitive to the cancellation process are not yet understood. To increase our understanding of the roles of plastic versus nonplastic cells in the cancellation process, we built a neural network model based on the known ELL anatomy.

Figure 6A illustrates the anatomical relationship between ELL pyramidal cells and the source of electrosensory feedback, the n. praeeminentialis dorsalis (nPd). Only the indirectly descending feedback pathway is shown for simplicity. The nPd multipolar cells (Mp) receive input from the pyramidal cells and project to the caudal cerebellum (posterior eminentia granularis, EGp), the granule cells (Gr) of which project to the ELL dorsal molecular layer. The axons of the Gr cells, parallel fibers, provide excitatory synaptic input to the pyramidal cell apical dendrites as well as disynaptic inhibitory input via the stellate cells (St). Since the nPd multipolar cells, as well as other nPd efferents, ultimately receive their synaptic inputs from the ELL pyramidal cells, the adaptive plasticity could alter the activity pattern of nPd efferents. Thus, characteristics of the plasticity itself could depend on the degree to which nPd efferent neurons receive input from the plastic versus nonplastic cells.

The model network is composed of a sensory neuron layer (e.g., pyramidal cells) modeled as leaky integrate-and-fire neurons coupled to feedback kernels as depicted in Figure 6B (see Experimental Procedures). Sensory input excites and inhibits E and I cells, respectively. For simplicity, it was assumed that the population consisted of only plastic (p) and nonplastic (np) types, corresponding to the cells with the largest and smallest apical dendrites. These cells project to higher brain centers representing the combined nPd and EGp circuitry, and the relative proportions of plastic and nonplastic inputs to the feedback kernels are governed by the factors c and $1 - c$, respectively. Thus, the higher brain centers receive input exclusively from nonplastic cells if $c = 0$ and exclusively from plastic cells if $c = 1$.

The higher brain center, Σ_E, sums the contributions from the E cells, and Σ_I sums the contributions from the I cells. Σ_E and Σ_I both project back to pyramidal cells such that Σ_E excites/inhibits I_P/E_P cells and Σ_I inhibits/excites I_P/E_P cells, respectively. Thus, both plastic cell categories receive descending inhibition and excitation in phase and antiphase, respectively, with ascending excitation due to receptor afferent input. Apical dendritic synaptic weights of plastic cells are allowed to vary in time in order to implement synaptic plasticity. The evolution of excitatory synaptic weights is governed by an anti-Hebbian learning rule, while inhibitory weights are governed by an inverse rule as described by Nelson and Paulin (1995). Although, in reality, cells with the smallest apical dendrites also receive feedback input, their feedback gain is fixed in agreement with the observation that they are not plastic. This allows us to absorb this "constant" feedback term into the input to the nonplastic cells.

The raster plots of Figures 7A1–7A4 contrast the behavior of a typical plastic E cell with simulations in which the ratio of plastic to nonplastic input to the feedback kernels (c value) was varied. Simulated responses to the initial global stimulus (Figures 7A2–A4 [G1]) were allowed to come to an equilibrium state where cancellation of the global stimulus was relatively complete and synaptic weights adopted a stable value. The local stimulus was then applied only to the simulated cells under study for 100 s as in the in vivo experiments. As in the case of the in vivo experiments, the initial strong responses to the G+L stimulus shows that the system

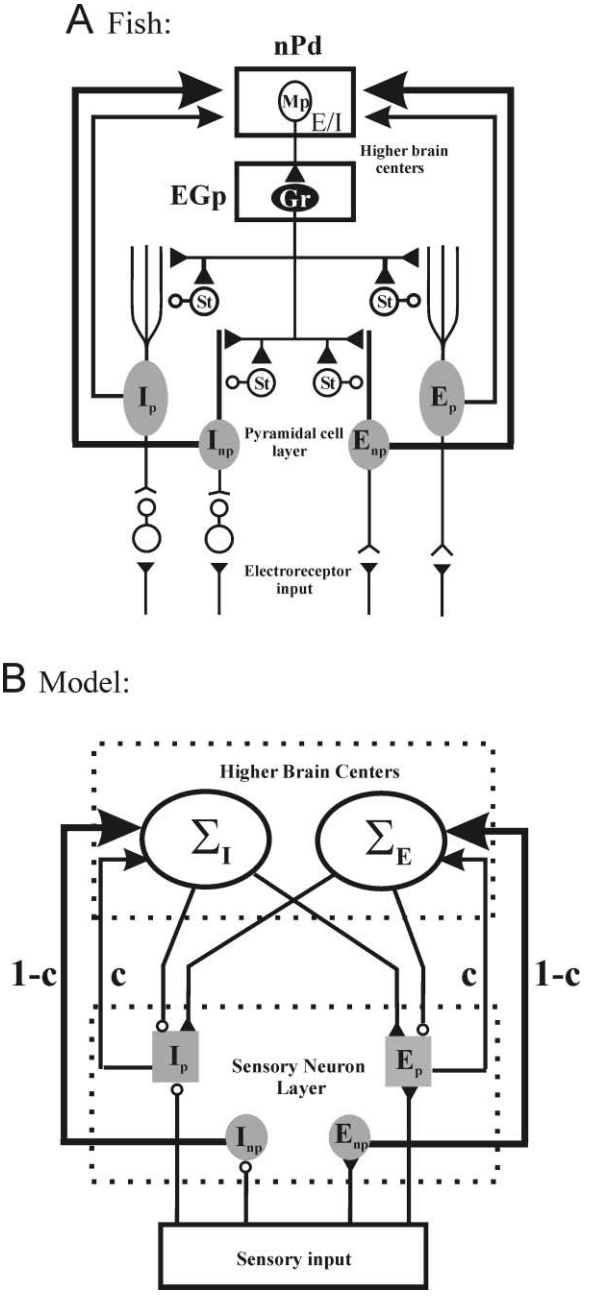

Figure 6. Diagramatic Comparison of Electrosensory Lateral Line Lobe Circuitry and the Numerical Model Used to Simulate Adaptive Plasticity of Pyramidal Cells

(A) Simplified diagram of ELL circuitry showing electroreceptor input to E (E_p, E_{np}) and I (I_p, I_{np}) cells of plastic (p) and nonplastic (np) types. These cells project to higher centers including the n. praeeminentialis dorsalis (nPd), which is the source of direct (not shown) and indirect feedback to the ELL. Praeeminentialis multipolar cells (Mp) project to granule cells (Gr) of the posterior eminentia granularis (EGp), and the axons of these (cerebellar parallel fibers) provide feedback excitation as well as disynaptic inhibition, via stellate cells (St), to the pyramidal cell apical dendrites.

(B) Model consisting of pyramidal cells of the same four types that project to feedback kernels, Σ_E and Σ_I, and receive both excitatory and inhibitory feedback input from these kernels. The parameter, c, ranges from 0 to 1 and specifies the ratio of plastic to nonplastic pyramidal cell output that projects to the feedback kernels. See Experimental Procedures for model description.

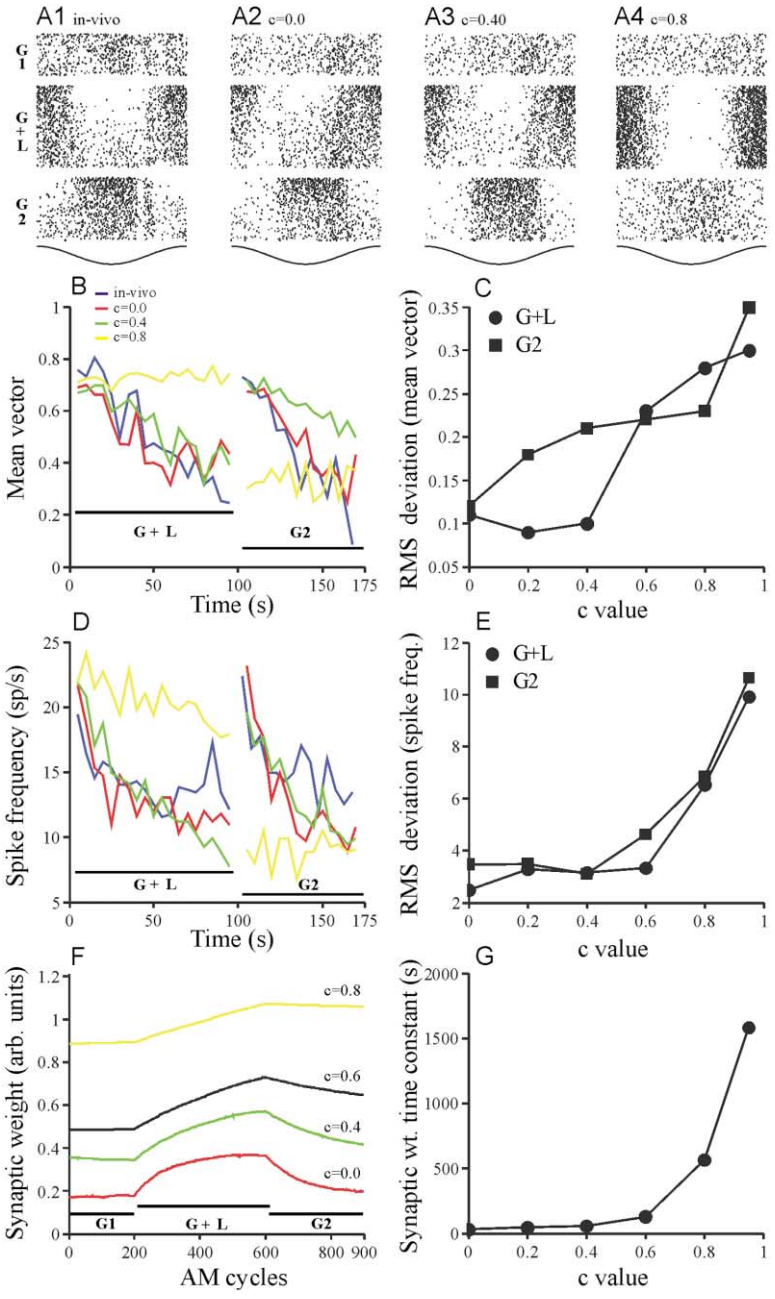

Figure 7. Comparisons of In Vivo and Modeled Pyramidal Cell Adaptive Plasticity

(A1) In vivo responses of an E cell during global stimulation (G1), global plus local stimulation (G+L), followed by global stimulation (G2).

(A2–A4) Simulated pyramidal cell responses to the same stimulation paradigm with different ratios of plastic to nonplastic input to the feedback kernels (c value).

(B) Comparisons of the time courses of plasticity during global plus local stimulation (G+L) and decay of negative image responses during global stimulation (G2) measured as phase histograms mean vectors computed over consecutive 5 s epochs.

(C) Plots of goodness of fit (rms deviations) of mean vectors of simulated responses to in vivo responses as a function of c value.

(D) Comparisons of the time courses of spike frequency changes during global plus local stimulation (G+L) and during decay of negative image responses (G2) measured over 5 s epochs.

(E) Plots rms deviations of simulated spike frequency from in vivo spike frequency as a function of c value.

(F) Plots of changes in synaptic weight (W_{EI}) versus time for the indicated c values.

(G) Plots of time constants of synaptic weight change as a function of c.

preserves sensitivity to novel stimuli even though responses to the global, nonnovel stimulus have been canceled. The local stimulus was then removed, revealing negative image responses to the global stimulus alone (Figures 7A2–7A4 [G2]).

Both the ability of the cell to adaptively cancel the G+L stimulus as well as the magnitude and duration of the negative image responses are sensitive to the value of c (compare middle and lowest raster segments of Figures 7A2–7A4). Mean vectors were computed for consecutive 5 s epochs over the 100 s of the G+L stimulus and the subsequent global stimulus alone (Figure 7B). The goodness-of-fit of the simulations to the in vivo data was then estimated by calculating the root-mean-square (rms) differences between simulation results for each value of c and the in vivo data. The rate and extent of cancellation of responses to the G+L stimulus most closely match the in vivo data with c less than about 0.4 (Figure 7C, circles). Increasing c to 0.6 results in significant loss of the cancellation, and with c equal to 0.8, cancellation is virtually absent (Figure 7A4). The magnitude and time course of the negative image responses following removal of the local stimulus are well matched to the in vivo data only with $c = 0$, i.e., when feedback is exclusively driven by nonplastic cells (Figures 7A2–7A4 [G2] and 7B [G2], red trace). With higher values of c, the time course of negative image decay is prolonged (Figure 7B [G2], green trace) resulting in larger RMS deviations (Figure 7C, squares). When the output of plastic cells dominates input to the feedback kernel,

only weak negative image responses are generated (Figures 7A4 [G2] and 7B, yellow).

Spike frequency was also monitored throughout actual and simulated experiments. In vivo data (Figure 7D, blue) show an increase in firing rate that adapts in response to G+L stimulation and a similar transient increase when the stimulus is returned to global alone. Changes in spike frequency for simulations with c ranging from 0 to 0.4 match the in vivo data well, but as c values increase beyond 0.6, the rms deviations (Figure 7E) indicate growing mismatches. The transient spike frequency increases associated with the switches from global alone to G+L stimulation and the switch back to global are responses to presentations of novel stimuli. With $c = 0.8$, these changes are drastically altered (Figure 7D [G+L and G2], yellow). Thus, having the feedback input predominantly driven by plastic pyramidal cells not only results in deterioration of the adaptive cancellation but also removes the transient changes in spike frequency that normally indicate the appearance of a novel stimulus.

Examples of the time course of changes in an example synaptic weight, the descending excitatory input to I cells (W_{EI}, see Experimental Procedures), are shown in Figure 7F, and two important attributes of these weights depend on c. First, the efficiency with which the cells are able to cancel the initial global stimulus decreases with increasing c values; synaptic weights are forced to higher values before they become stable. Consequently, the weights must attain still higher values in order to achieve cancellation of the G+L stimuli. Second, the time course of weight changes during cancellation of the G+L stimuli is prolonged as c increases. The plot of the synaptic weight change time constant as a function of c (Figure 7G) summarizes this dependency. As the ratio of plastic to nonplastic inputs to the feedback kernels increases, the magnitude of weight changes necessary to cancel a given input increases, as does the time necessary to achieve a given degree of cancellation.

Overall, these simulations most closely match the experimental data when the input to the feedback kernel is exclusively from the nonplastic cells. Increasing the proportion of input to the feedback kernel (nPd) carried by plastic cells compromises the efficiency of the cancellation processes by forcing much larger changes in synaptic weight, by slowing the rate at which cancellation proceeds, and by altering the transient changes in firing frequency due to the onset of novel stimuli. These modeling results predict that the ELL efferent projection to the nPd should be predominantly, if not exclusively, composed of axons of the nonplastic pyramidal cells, which are identifiable by their small apical dendrites.

Nonplastic Pyramidal Cells Project to the n. praeeminentialis

Earlier studies, using horseradish peroxidase transport, identified the midbrain torus semicircularis (TS) and the n. praeeminentialis dorsalis as the only targets of ELL pyramidal cell axons (Maler et al., 1982) and raised the possibility that a subset of the cells having the smallest apical dendrites preferentially projected to the nPd (Bastian and Courtright, 1991). These projections were reexamined using the more sensitive Neurobiotin technique and confocal imaging. Injections of Neurobiotin into the nPd strongly labeled only cells with small apical dendrites and somata deep within the pyramidal cell layer (Figure 8A, arrows). These cells were identical to the nonplastic small-dendrite cells identified by intracellular labeling (Figure 3B9). The apical dendrites of these cells ramified within the ventral molecular layer and the deeper half of the dorsal molecular layer. Torus injections resulted in intense labeling of a diverse cell population with somata distributed throughout the pyramidal cell layer. This population included cells with large apical dendrites traversing the full extent of the molecular layers (Figure 8B). Torus injections also filled deep cells; however, their small dendrites were only weakly labeled (Figure 8D, arrows). Torus and nPd injections also produced labeling in small nonbasilar cells located ventrally within the pyramidal cell layer (Figures 8C and 8D, asterisks), likely corresponding to the nonplastic I cells.

Pressure injections of Neurobiotin to nPd also resulted in very weak labeling of a few superficial pyramidal cells (Figure 8C, arrow). However, in these cases, the injection pipette passed through the TS, and low levels of Neurobiotin were observed to have diffused into that structure. We conclude that the ELL projection to the nPd is mainly, and perhaps entirely, from deep pyramidal cells, as predicted by our computational analysis. In contrast, all morphological variants of pyramidal cells (plastic and nonplastic) project to the torus semicircularis.

Discussion

The presence of nonplastic and plastic cells embedded in a feedback network confers novel computational properties on the network that are not apparent from the physiology of these cells considered in isolation. We have demonstrated that the ability of the plastic cells to attenuate responses to redundant patterns of sensory input, without compromising sensitivity to novel stimuli, requires feedback information encoded by nonplastic cells. The patterns of input that can be cancelled are of low spatial and temporal frequency (Bastian, 1996a), and in principle this could be accomplished via response adaptation utilizing feedforward mechanisms such as balanced antagonistic center-surround receptive fields and common mode rejection. The plastic cells do have antagonistic center surround receptive fields (Bastian et al., 2002); however, earlier studies demonstrated that functional feedback to the apical dendrites is necessary for adaptive cancellation (Bastian, 1996a); thus, feedforward mechanisms alone are not sufficient. In addition, simulation studies of a similar system verified that cancellation mediated solely by common-mode rejection mechanisms is very sensitive to mismatches of the signals provided by the antagonistic receptive field components and that addition of a similar adaptive filtering mechanism resulted in marked improvements in cancellation (Nelson and Paulin, 1995). The adaptive nature of the mechanism enables the system to perform well under a wide range of conditions including during growth and development as well as following events that damage or otherwise alter receptive field characteristics.

We have recently shown that unlike spatially redun-

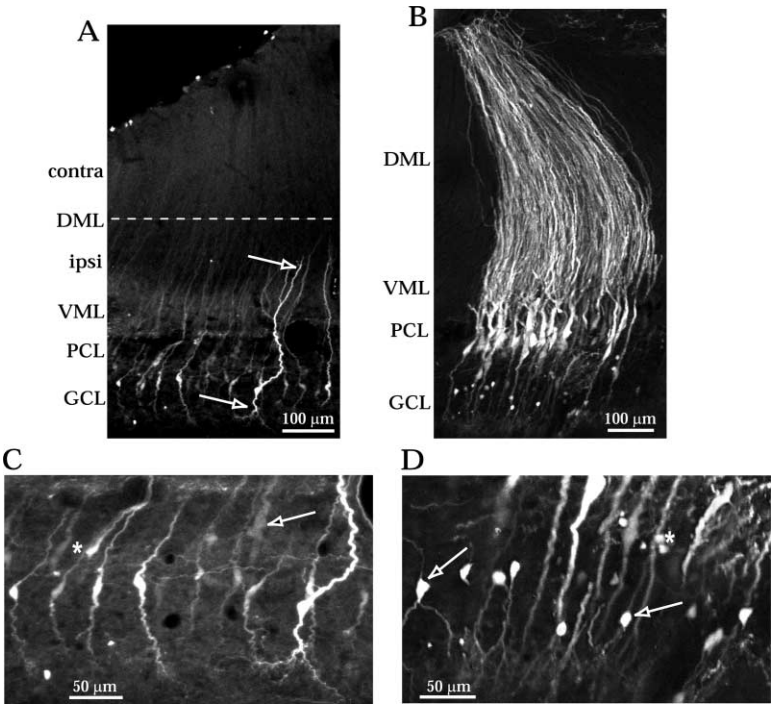

Figure 8. Confocal Images of Retrogradely Labeled ELL Pyramidal Cells

(A) nPd injections label small-dendrite pyramidal cells within the granule cell layer. Apical dendrites extend through the VML and ramify in the lower half of the DML (upper arrow) and basilar dendrites ramify within the deep fiber layer (lower arrow). The dashed line demarcates the boundary between the lower DML (ipsi, input from ipsilateral EGp) and the upper DML (contra, input from contralateral EGp) (Sas and Maler, 1987). Weak anterograde labeling is also seen within the VML.

(B) TS injections strongly label superficial and intermediate pyramidal cells; their dendrites traverse the full dorsoventral extent of the molecular layers. Smaller cells within the granule cell layer are also labeled.

(C) Higher magnification of the small cells of (A); arrow points to a weakly labeled more superficial pyramidal cell. Asterisk indicates small retrogradely labeled deep nonbasilar pyramidal cell.

(D) Higher magnification of the cells of (B); arrows indicate deep cells with basilar dendrites and asterisk indicates deep nonbasilar cell. DML, dorsal molecular layer; GCL, granule cell layer; PCL, pyramidal cell layer; VML, ventral molecular layer.

dant stimuli of low temporal frequency, spatially identical stimuli of high frequency are transmitted well by the plastic cells (Chacron et al., 2003). If feedforward common mode rejection was a significant component of the mechanism described here, we would expect such signals to be attenuated as well. The adaptive nature of the feedback cancellation mechanism may also provide a flexible method of reducing spatial redundancy in a frequency-dependent manner; such selectivity may not be possible with a classic antagonistic center-surround mechanism.

Rather than eliminating redundancy at early stages in sensory processing as originally suggested by Attneave (1954) and Barlow (1961), a more effective strategy may be to encode redundant or predictable information via a separate channel (Barlow, 2001). This information, which can be considered noise in some contexts, can be removed from specific channels by suitable network operations, thereby enhancing sensitivity to novel events. Preservation of the redundant information in independent channels may also enable the animal to exploit the predictable components of the stimulus for other critical operations. The adaptive plasticity and network architecture described here accomplishes these tasks; spatially redundant (global) information is preserved by the nonplastic cells' projection to the TS while the plastic cells reject global stimulus components. Important communication behaviors of many weakly electric fish, the jamming avoidance response (JAR), and the production of chirps during mating and agonistic encounters require that the fish analyze the *predictable* beats produced by the interfering EODs (Heiligenberg, 1991). This would not be possible if all ELL neurons rejected these periodic stimuli. ELL pyramidal cells also preserve their responses to electrolocation targets despite significant decreases in overall EOD amplitude. This gain control mechanism (Bastian, 1986b) requires that the steady-state amplitude of the EOD be known, and this information is also encoded by the nonplastic pyramidal cells (Bastian and Courtright, 1991). Thus, the nonplastic cells provide information critical for efficient adaptive cancellation as well as for other important electrosensory functions.

Although the mechanisms responsible for the variations in plasticity seen across the pyramidal cell population are not fully understood, analysis of membrane potential changes demonstrates that the small-dendrite cells' lack of plasticity is not due to ineffective dendritic inputs. Instead, differences in the postsynaptic cells' receptor characteristics and intracellular signaling systems probably underlie this variability. This plasticity requires functional NMDA receptors (J.B., unpublished observations; Lewis and Maler, 2003) and is Ca^{2+} dependent (Bastian, 1998), and cells with different dendritic structures vary with respect to Ca^{2+}-dependent signaling molecules. Large-dendrite cells strongly express both IP3 and ryanodine receptor immunoreactivity. Cells with intermediate dendritic size express only ryanodine immunoreactivity, while cells with the smallest dendrites express neither (Zupanc et al., 1992; Berman et al., 1995).

All ELL pyramidal cells express the NR1 subunit of the NMDA receptor (Bottai et al., 1997, 1998), and feedback pathway EPSPs to these cells have a prominent NMDA receptor component (Berman et al., 2001). The NR2B subunit of the NMDA receptor of *Apteronotus* has recently been identified and shown to be highly homologous with mammalian NR2B, including the C-terminal domains and CaMKII binding sites linked to the expression of synaptic plasticity (Harvey-Girard and Dunn, 2003). The NR2B subunit is also differentially expressed among ELL pyramidal cells, with highest levels being

found in cells with the most extensive dendrites, significantly lower levels in cells with intermediate dendrites, and undetectable in cells having the smallest dendrites (E. Harvey-Girard, personal communication). The NR2B subunit appears to be an essential component of synaptic plasticity in mammalian cortical pyramidal cells (Krapivinsky et al., 2003). We therefore hypothesize that Ca^{2+} entry via NMDA receptors plus Ca^{2+}- and NR2B-associated signaling cascades are critical constituents of the molecular machinery underlying pyramidal cell adaptive plasticity; further, we propose that lack of the NR2B subunit and Ca^{2+} signaling proteins accounts for the nonplastic nature of the small-dendrite cells. Additional in vitro studies involving direct manipulation of these intracellular signaling systems are needed to verify this hypothesis.

Cortical pyramidal cells also display enormous variation in dendritic structure (Haüsser and Mel, 2003), and significant numbers of these neurons also lack Ca^{2+}-dependent signaling proteins (CaMKIIα; Jones et al., 1994) critical for long-term plasticity. Physiological studies demonstrate that large numbers of cortical pyramidal cells are not plastic (Hardingham et al., 2003). The relationships between the physiologically nonplastic cortical pyramidal cells, those lacking components of Ca^{2+}-dependent signaling systems, and dendritic structure remain to be established, as does the computational consequences of having both plastic and nonplastic pyramidal cells in cortex.

Experimental Procedures

The weakly electric fish *Apteronotus leptorhynchus* was used in these studies. Fish were housed in groups of 3 to 10 in 150 liter tanks at 26°C to 28°C with water resistivity from 2000 to 5000 Ω·cm. Experiments were carried out in a 39 $\times$ 44 $\times$ 12 cm deep Plexiglas aquarium with water recirculated from the animal's home tank. Animals were artificially respirated with a continuous water flow of 10 ml/min. Surgical techniques were the same as described previously (Bastian, 1996a, 1996b); all procedures were in accordance with the University of Oklahoma animal care and use guidelines and the University of Ottawa Animal Care Committee.

Recording and Single Cell Reconstructions

Extracellular single unit recordings were made with metal-filled micropipettes (Frank and Becker, 1964). Recording sites, determined from surface landmarks and recording depths, were limited to the lateral and centrolateral ELL segments. Intracellular recordings were made with sharp micropipettes filled with 2% neurobiotin in 1 M KCl (pH 7.6, 0.05 M tris). Electrode impedance ranged from 70 to 150 MΩ. Extracellularly recorded spikes were detected with window discriminators and time stamped (CED 1401-plus hardware and SpikeII software, resolution = 0.1 ms; Cambridge Electronic Design, Cambridge, UK). Intracellularly recorded spikes were detected in the same manner, and membrane potential was A-to-D converted at 10 kHz. Cells were filled by passing positive DC offset sinusoidal currents ranging from 0.5 to 2 nA for from 2 to 5 min. Following 1 hr survival time, animals were deeply anesthetized (tricain methane sulfonate, MS-222), perfused with phosphate-buffered saline (PBS, pH 7.4), followed by 4% paraformaldehyde in phosphate buffer, followed by 4% paraformaldehyde-30% sucrose in PB. Brains were removed, postfixed overnight in paraformaldehyde-sucrose, then embedded in gelatin (10% in 30% sucrose). After overnight fixation, embedded brains were sectioned at 60 μm and incubated overnight for peroxidase histochemistry (Vectastain Elite ABC, Vector Labs), and labeling was visualized with Vector-SG. Reconstructions were produced from camera lucida drawings. Apical dendritic lengths were measured as the summed linear extent of all branches with a MetaMorph (Universal Imaging Corp.) image analysis system.

Tract Tracing Studies

Fish were anaesthetized with 0.2% MS-222. For the torus semicircularis (TS) injections, the rostral cerebellum was lifted and a glass electrode with a clump of Neurobiotin (Vector Laboratories, Burlingame, CA) at its tip was inserted into the TS from its rostral aspect and left in place for about 10 s (n = 3). Similar injections into the nucleus praeminentialis dorsalis (nPd) were made from its lateral aspect at the surface of the brain (n = 3) (Maler et al., 1991; atlas level 4). Glass micropipettes (broken to 20 μm) were backfilled with 10% Neurobiotin in 0.1 M potassium methylsulfate and lowered into nPd through the TS (Maler et al., 1991; atlas level T5). Pressure injections were made using a Picospritzer (n = 4). After 24 hr survival, the fish were deeply anesthetized and perfused with 4% paraformaldehyde, 0.1% gluteraldehyde, 0.2% picric acid in 0.1 M PBS (pH 7.4). The brains were removed and fixed overnight (without glutaraldehyde, 4°C), then sectioned at 80 μm. Free-floating sections were washed and incubated in Streptavidin conjugated to CY3 (1:100 in 1% normal goat serum, 1% BSA, 0.3% Triton-X, and PBS) for 48 hr. Sections were then washed, mounted, and coverslipped.

A series of 15–20 confocal images were obtained at a Z increment of 4 μm through clusters of retrogradely labeled cells (Zeiss LSM410) using 10$\times$ or 20$\times$ lenses. The stack of images was summed (NIH Image software) and the contrast optimized (Adobe Photoshop); no further image enhancements were made.

Stimulation

The electric organ of *Apteronotus* consists of modified motoneurons; hence, it remains intact during the neuromuscular blockade used in these experiments. The EOD waveform was measured via Ag||AgCl wire electrodes positioned near the animal's head and tail (gain = 1000, filters set at 0.3 and 3 kHz, DAM50 amplifier, World Precision Instruments, Sarasota, FL). Electrosensory stimuli consisted of amplitude modulations of the normal EOD produced by adding an EOD mimic to the ongoing discharge. The EOD mimic consisted of a train of single sinusoidal waveforms each triggered at the zero-crossing of the head to tail EOD record, and hence, the mimic remained synchronized to the animal's own discharge. To generate time-varying EOD AMs, the mimic was multiplied (MT3 multiplier, Tucker-Davis Technologies, Gainesville, FL) by a DC offset 4 Hz sine wave. The resulting signal was passed through a step attenuator for controlling amplitude, isolated from ground (WPI A395 linear stimulus isolator), then applied to the animal with either of two geometries. With global geometry the stimulus was applied via Ag||AgCl electrodes approximately 19 cm lateral to either side of the fish. This results in a relatively homogeneous change in EOD amplitude over the body surface on a given side of the fish. The standard global stimulus had peak-to-peak amplitude of 300 μV/cm. With the second, local geometry, stimulus signals were generated as described above but delivered via a small stimulus dipole (76 μm stainless steel wires insulated except for their tips; tip spacing = 8 mm). This dipole was carried by a computer-controlled 3-axis positioning device that allowed placement of the dipole at any selected site on, or lateral to, the skin surface. The resulting changes in EOD amplitude were measured within each cell's receptive field center with a small dipole pair of Ag||AgCl electrodes (2 mm tip spacing) oriented perpendicular to the animal's skin and amplified with a WPI DAM50 preamplifier (gain = 10,000; filters at 0.3 and 3 kHz) and A-to-D converted at 10 kHz.

The standard local stimulus produced a peak-to-peak AM approximately 5-fold greater than that due to the global stimulus. Responses to sinusoidal amplitude modulation stimuli (SAM) were accumulated as phase histograms and responses were quantified as the vector strength (Batschelet, 1981), which ranges from 0, when there is no phase relationship between the stimulus and response, to 1 with perfect phase-locking. Micropressure injection of the non-NMDA glutamate antagonist CNQX (6-cyano-7-nitroquinoxaline-2,3-dione) was accomplished as described by Bastian (1993).

Modeling

Model Description

We model the ELL pyramidal cell layer as a leaky integrate-and-fire (LIF) neuron network (Dayan and Abbott, 2001) comprising 4N

neurons. The membrane potential of neuron I is denoted by V_i. When V_i crosses a threshold θ, a spike is said to occur and V_i is reset to a value V_{reset} and is kept there during the absolute refractory period T_r. 2N neurons are nonplastic, with N having E type responses (E_{np}) and the other half having I type responses (I_{np}). The other 2N neurons are plastic, with half having E type (E_p) and half having I type (I_p) responses. The membrane potential V_i for nonplastic neurons is governed by the following stochastic equation:

$$C\frac{dV_i}{dt} = -g_{leak}(V_i - E_{leak}) + I_{oi} + \xi_i(t) + s_i I_i(t),$$

where g_{leak} is the leak conductance, C is the membrane capacitance, and E_{leak} is the leak reversal potential. We have $s_i = 1$ if neuron i has E type response and $s_i = -1$ if it has I type response. I_{0i} is a constant baseline current. $I_i(t)$ is the time varying stimulus to neuron i, and $\xi_i(t)$ is a Gaussian random variable of zero mean and standard deviation σ that represents noise present in neuron i. We assume that the noise sources are independent and identically distributed among the neurons.

The membrane potential V_i for plastic neurons is governed by

$$C\frac{dV_i(t)}{dt} = -g_{leak}[V_i(t) - E_{leak}] + I_{oi} + \xi_i(t) + s_i[I_i(t) - w_{Ei}(t)\Sigma_E(t) + w_{Ii}(t)\Sigma_I(t)],$$

which includes feedback terms modeled using an approach similar to that used in Doiron et al. (2003), where the higher brain centers are represented by summation kernels, respectively, given by

$$\Sigma_E(t) = (1 - c)\sum_{j\in E_{np}}\sum_{m=1}^{M_j(t)} I(t - t_{jm}) + c\sum_{j\in E_p}\sum_{m=1}^{M_j(t)} I(t - t_{jm})$$

$$\Sigma_I(t) = (1 - c)\sum_{j\in I_{np}}\sum_{m=1}^{M_j(t)} I(t - t_{jm}) + c\sum_{j\in I_p}\sum_{m=1}^{M_j(t)} I(t - t_{jm})$$

Each kernel receives a contribution from the nonplastic and plastic cells. These contributions are controlled by the parameter c. Thus, if c = 0.2, then 20% of the input to these kernels comes from the plastic cells and 80% from the nonplastic cells. In each contribution, each spike from neuron j is converted to a double exponential function I (Dayan and Abbott, 2001) to mimic synaptic PSP's given by

$$I(t) = \exp\left[-\frac{t}{\tau_1}\right] - \exp\left[-\frac{t}{\tau_2}\right],$$

where τ_1 and τ_2 are time constants. The contribution is done over the m spike times t_{jm} of neuron j up to its spike count $M_j(t)$ at time t. We neglect axonal transmission delays since these are very small relative to the period of the low-frequency stimuli used (4 Hz). We model synaptic plasticity for pyramidal cells by letting the synaptic weights w_{Ei} and w_{Ii} evolve in time according to the following differential equations (Nelson and Paulin, 1995):

$$\frac{dw_{Ei}(t)}{dt} = -s_i\eta[r_i(t) - \rho_i(t)][\Sigma_E(t) - \rho_E(t)]$$

$$\frac{dw_{Ii}(t)}{dt} = -s_i\eta[r_i(t) - \rho_i(t)][\Sigma_I(t) - \rho_I(t)],$$

where η is the learning rate and $r_i(t)$ is the time varying firing rate of neuron i obtained by convolving the spike train with a Gaussian filter of standard deviation 10 ms. Moreover, we have:

$$\frac{d\rho_i(t)}{dt} = \frac{r_i(t) - \rho_i(t)}{\tau}$$

$$\frac{d\rho_E(t)}{dt} = \frac{\Sigma_E(t) - \rho_E(t)}{\tau}$$

$$\frac{d\rho_I(t)}{dt} = \frac{\Sigma_I(t) - \rho_I(t)}{\tau}.$$

Thus, the ρ variables are low-pass filtered versions of the firing rates and feedback kernels with time constant τ and represent their "steady-state" values on the time scale τ, respectively. For all the simulations, we used N = 50, g_{leak} = 0.15 nS, C = 0.75 nF, $E_{leak} = -70$ mV, $V_{reset} = -80$ mV, $\theta = -35$ mV, σ = 3.16 nA, τ_1 = 4 ms, τ_2 = 1 ms, τ = 1 s, and $\eta = 1.25 \times 10^{-4}$ s^{-1}. To model the differences in firing rates seen for NP and P cells, we used I_{0i} = 3.5 nA and I_{0i} = 3.0 nA for each group, respectively.

Simulated Plasticity Experiment

The global stimulus was modeled as a sinusoidal modulation of the input current, with f = 4 Hz as in the in vivo experiments, for all neurons in the network. We modeled the addition of the local stimulus by modifying the amplitude of the input to only one member of each group E_{np}, E_p, I_p, and I_{np}. Thus, cells not receiving the extra local stimulus had $I_i(t) = s_i$ A $\sin(2\pi ft)$ during the course of the simulated plasticity experiment while cells receiving the local stimulus had

$$\begin{aligned} I_i(t) &= s_i[A + \Delta A]\sin[2\pi ft) \quad \text{if } 50 < t < 150 \text{ sec} \\ I_i(t) &= s_i A\sin(2\pi ft) \quad \text{otherwise} \end{aligned}.$$

We chose A = 2.7 nA and ΔA = 2.5 nA.

Acknowledgments

This work was supported by grants from the NIH (J.B.) and the CIHR (L.M.).

Received: September 17, 2003
Revised: November 25, 2003
Accepted: January 20, 2004
Published: March 3, 2004

References

Attneave, F. (1954). Informational aspects of visual perception. Psychol. Rev. *61*, 183–193.

Bannister, N.J., and Larkman, A.U. (1995). Dendritic morphology of CA1 pyramidal neurons from the rat hippocampus. I. Branching patterns. J. Comp. Neurol. *360*, 161–171.

Barlow, H.B. (1961). The coding of sensory messages. In Current Problems in Animal Behavior, W.H. Thorpe and O.L. Zangwill, eds. (Cambridge: Cambridge University Press), pp. 331–360.

Barlow, H. (2001). Redundancy reduction revisited. Network *12*, 241–253.

Bastian, J. (1986a) Electrolocation: behavior anatomy and physiology. In Electroreception, T.H. Bullock and W. Heiligenberg, eds. (New York: Wiley), pp. 577–612.

Bastian, J. (1986b). Gain control in the electrosensory system mediated by descending inputs to the electrosensory lateral line lobe. J. Neurosci. *6*, 553–562.

Bastian, J. (1993). The role of amino acid neurotransmitters in the descending control of electroreception. J. Comp. Physiol. [A] *172*, 409–423.

Bastian, J. (1995). Pyramidal cell plasticity in weakly electric fish: a mechanism for attenuating responses to reafferent electrosensory inputs. J. Comp. Physiol. [A] *176*, 63–78.

Bastian, J. (1996a). Plasticity in an electrosensory system. I. General features of a dynamic sensory filter. J. Neurophysiol. *76*, 2483–2496.

Bastian, J. (1996b). Plasticity in an electrosensory system. II. Postsynaptic events associated with a dynamic sensory filter. J. Neurophysiol. *76*, 2497–2507.

Bastian, J. (1998). Modulation of calcium-dependent postsynaptic depression contributes to an adaptive sensory filter. J. Neurophysiol. *80*, 3352–3355.

Bastian, J. (1999). Plasticity of feedback inputs in the apteronotid electrosensory system. J. Exp. Biol. *202*, 1327–1337.

Bastian, J., and Courtright, J. (1991). Morphological correlates of pyramidal cell adaptation rate in the electrosensory lateral line lobe of weakly electric fish. J. Comp. Physiol. [A] *168*, 393–407.

Bastian, J., and Nguyenkim, J. (2001). Dendritic modulation of burst-like firing in sensory neurons. J. Neurophysiol. *85*, 10–22.

Bastian, J., Chacron, M.J., and Maler, L. (2002). Receptive field organization determines pyramidal cell stimulus-encoding capability and spatial stimulus selectivity. J. Neurosci. *22*, 4577–4590.

Batschelet, E. (1981). Circular Statistics in Biology (New York: Academic Press).

Bell, C.C. (2001). Memory-based expectations in electrosensory systems. Curr. Opin. Neurobiol. *11*, 481–487.

Bell, C.C., Bodznick, D., Montgomery, J., and Bastian, J. (1997). The generation and subtraction of sensory expectations within cerebellum-like structures. Brain Behav. Evol. *50*, 17–31.

Berman, N.J., Hincke, M.T., and Maler, L. (1995). Inositol 1,4,5-trisphosphate receptor localization in the brain if a weakly electric fish (*Apteronotus leptorhynchus*) with emphasis on the electrosensory system. J. Comp. Neurol. *361*, 512–524.

Berman, N.J., Dunn, R.J., and Maler, L. (2001). Function of NMDA receptors and persistent sodium channels in a feedback pathway of the electrosensory system. J. Neurophysiol. *86*, 1612–1621.

Bottai, D., Dunn, R.J., Ellis, W., and Maler, L. (1997). N-methyl-D-aspartate receptor 1 mRNA distribution in the central nervous system of the weakly electric fish *Apteronotus leptorhynchus*. J. Comp. Neurol. *389*, 65–80.

Bottai, D., Maler, L., and Dunn, R.J. (1998). Alternative RNA splicing of the NMDA receptor NR1 mRNA in the neurons of the teleost electrosensory system. J. Neurosci. *18*, 5191–5202.

Chacron, M.J., Doiron, B., Maler, L., Longtin, A., and Bastian, J. (2003). Non-classical receptive field mediates switch in a sensory neuron's frequency tuning. Nature *423*, 77–81.

Dayan, P., and Abbott, L.F. (2001). Theoretical Neuroscience: Computational and Mathematical Modeling of Neural Systems (Cambridge, MA: MIT University Press).

Doiron, B., Laing, C., Longtin, A., and Maler, L. (2002). Ghostbursting: a novel neuronal burst mechanism. J. Comput. Neurosci. *12*, 5–25.

Doiron, B., Chacron, M., Maler, L., Longtin, A., and Bastian, J. (2003). Inhibitory feedback required for network oscillatory responses to communication but not prey stimuli. Nature *431*, 539–543.

Frank, K., and Becker, M.C. (1964). Microelectrodes for recording and stimulation. In Physical Techniques in Biological Research, vol. *5*, part A. (New York: Academic Press), pp. 23–84.

Hagedorn, M., and Heiligenberg, W. (1985). Court and spark: signals in the courting and mating of gymnotid fish. Anim. Behav. *33*, 254–265.

Hardingham, N., Glazewski, S., Pakhotin, P., Mizuno, K., Chapman, P.F., Giese, K.P., and Fox, K. (2003). Neocortical long-term potentiation and experience-dependent synaptic plasticity require a-calcium/calmodulin-dependent protein kinase II autophosphorylation. J. Neurosci. *23*, 4428–4436.

Harvey-Girard, E., and Dunn, R.J. (2003). Excitatory amino acid receptors of the electrosensory system: the NR1/NR2B N-methyl-D-aspartate receptor. J. Neurophysiol. *89*, 822–832.

Haüsser, M., and Mel, B. (2003). Dendrites: bug or feature? Curr. Opin. Neurobiol. *13*, 372–383.

Haüsser, M., Spruston, N., and Stuart, G.J. (1999). Conclusion: the future of dendritic research. In Dendrites, M. Hausser, N. Spruston, and G.J. Stuart, eds. (New York: Oxford University Press), pp. 365–368.

Heiligenberg, W. (1991). Neural Nets in Electric Fish (Cambridge, MA: MIT Press).

Jones, E.G., Huntley, G.W., and Benson, D.L. (1994). Alpha calcium/calmodulin-dependent protein kinase II selectively expressed in a subpopulation of excitatory neurons in monkey sensory-motor cortex: comparison with GAD-67 expression. J. Neurosci. *14*, 611–629.

Koch, C., and Segev, I. (2000). The role of single neurons in information processing. Nat. Neurosci. *3*, 1171–1177.

Krapivinsky, G., Krapivinsky, L., Manasian, Y., Ivanov, A., Tyzio, R., Pellegrino, C., Ben-Ari, Y., Clapham, D.E., and Medina, I. (2003). The NMDA receptor is coupled to the ERK pathway by a direct interaction between NR2B and RasGRF1. Neuron *40*, 775–784.

Larkman, A., and Mason, A. (1990). Correlations between morphology and electrophysiology of pyramidal neurons in slices of rat visual cortex. I. Establishment of cell classes. J. Neurosci. *10*, 1407–1414.

Lemon, N., and Turner, R.W. (2000). Conditional backpropagation generates burst discharge in a sensory neuron. J. Neurophysiol. *89*, 1519–1530.

Lewis, J., and Maler, L. (2003). Synaptic dynamics on different timescales in a parallel fiber feedback pathway of the weakly electric fish. J. Neurophysiol., in press. Published online November 5, 2003. 10.1152/jn.00856.2003.

Maler, L. (1979). The posterior lateral line lobe of certain gymnotoid fish: quantitative light microscopy. J. Comp. Neurol. *345*, 323–363.

Maler, L., Sas, E.K., and Rogers, J. (1981). The cytology of the posterior lateral line lobe of high-frequency weakly electric fish (*Gymnotidae*): dendritic differentiation and synaptic specificity in a simple cortex. J. Comp. Neurol. *195*, 87–139.

Maler, L., Sas, E., Carr, C.E., and Matsubara, J. (1982). Efferent projections of the posterior lateral line lobe of gymnotiform fish. J. Comp. Neurol. *211*, 154–164.

Maler, L., Sas, E., Johnston, S., and Ellis, W. (1991). An atlas of the brain of the weakly electric fish *Apteronotus albifrons*. J. Chem. Neuroanat. *4*, 1–38.

Nelson, M.E., and MacIver, M.A. (1999). Prey capture in the weakly electric fish *Apteronotus leptorhynchus*: sensory acquisition strategies and electrosensory consequences. J. Exp. Biol. *202*, 1195–1203.

Nelson, M.E., and Paulin, M.G. (1995). Neural stimulations of adaptive reafference suppression in the elasmobranch electrosensory system. J. Comp. Physiol. [A] *177*, 723–736.

Sas, E., and Maler, L. (1987). The organization of afferent input to the caudal lobe of the cerebellum of the gymnotid fish *Apteronotus leptorhynchus*. Anat. Embryol. *177*, 55–79.

Saunders, J., and Bastian, J. (1984). The physiology and morphology of two types of electrosensory neurons in the weakly electric fish *Apteronotus leptorhynchus*. J. Comp. Physiol. [A] *154*, 199–209.

Segev, I., and London, M. (2000). Untangling dendrites with quantitative models. Science *290*, 744–750.

Zupanc, G.K.H., Airey, J.A., Maler, L., Sutko, J.L., and Ellisman, M.H. (1992). Immunohistochemical localization of ryanodine binding protein in the central nervous system of gymnotiform fish. J. Comp. Neurol. *325*, 135–151.